Analysis of Stokes flows by Carrera unified formulation

Alberto Varello, Alfonso Pagani*, Daniele Guarnera and Erasmo Carrera

Mul^2, Department of Mechanical and Aerospace Engineering, Politecnico di Torino, Corso Duca degli Abruzzi 24, 10129 Torino, Italy

Abstract. One-dimensional (1D) models of incompressible flows, can be of interest for many applications in which fast resolution times are demanded, such as fluid-structure interaction of flows in compliant pipes and hemodynamics. This work proposes a higher-order 1D theory for the flow-field analysis of incompressible, laminar, and viscous fluids in rigid pipes. This methodology is developed in the domain of the Carrera Unified Formulation (CUF), which was first employed in structural mechanics. In the framework of 1D modelling, CUF allows to express the primary variables (i.e., velocity and pressure fields in the case of incompressible flows) as arbitrary expansions of the generalized unknowns, which are functions of the 1D computational domain coordinate. As a consequence, the governing equations can be expressed in terms of fundamental nuclei, which are invariant of the theory approximation order. Several numerical examples are considered for validating this novel methodology, including simple Poiseuille flows in circular pipes and more complex velocity/pressure profiles of Stokes fluids into non-conventional computational domains. The attention is mainly focused on the use of hierarchical McLaurin polynomials as well as piece-wise nonlocal Lagrange expansions of the generalized unknowns across the pipe section. The preliminary results show the great advantages in terms of computational costs of the proposed method. Furthermore, they provide enough confidence for future extensions to more complex fluid-dynamics problems and fluid-structure interaction analysis.

Keywords: one-dimensional Stokes flows; Carrera unified formulation; higher-order models

1. Introduction

One-dimensional models in fluid-dynamics have attracted the interest of many researchers working in fluid-dynamics modelling, although the fundamental 3D nature of the phenomena considered. Many engineering applications, as a matter of fact, have a characteristic dimension which makes the problem as one-dimensional; for example, a river bed as well as a vessel represent a predominant direction for a river or for a blood flow, as suggested by Quarteroni *et al.* (2009) and Vreugdenhil (1998). Considering the computational hemodynamics as reference application, probably the first one-dimensional model belongs to Euler (1775), who derived the partial differential equations (PDEs) for mass and momentum conservations. From the mathematical point of view, this theory was later

---

*Corresponding author, E-mail: alfonso.pagani@polito.it

formalized by the Navier-Stokes set of equations that still represents a fundamental basis for fluids applications. More recently, the circulatory system was largely investigated by Fung in (Fung (1997)).

The simplification of a flow model from 3D to 1D does not represent an easy challenge, and probably, it may involve strong simplifications due to the presence of local phenomena related to turbulence, boundary conditions and other features. However, one-dimensional models of flows can take some advantages in terms of comprehension of complex networks, and in terms of computational costs. For this purpose, a coupling between FEM and spectral methods has been proposed by Perotto *et al.* (2017), whereas Formaggia *et al.* (2001) derived a 1D model of incompressible fluid by integrating the Navier-Stokes equations over each section normal to the longitudinal direction. On the other hand, a combination of isogeometric analyses with reduced order modeling techniques based on proper orthogonal decomposition (POD) was presented by Salmoiraghi *et al.* (2016). Similarly, Smith *et al.* (2002) developed a finite difference model of blood flow by integrating the axial velocity of the 3D equations, whereas Sherewin *et al.* (2003), carried out 1D analyses of a vascular network by using a spectral/hp element spatial discretization. Formaggia *et al.* (2003) proposed a family of 1D nonlinear systems for blood pulsing propagation in compliant arteries. Another branch of investigation is linked to the real-time solutions and active control of the PDEs in the case of complex fluids. The employment of CFD reduced models in such context has been analyzed by Ravindran *et al.* (2000) and Quarteroni and Rozza (2006).The one-dimensional approach is enhanced by its capability to be coupled with more refined models (i.e., 2D and 3D) in some delimited points of the domain, as proposed by Perotto *et al.* (2009) and by Formaggia *et al.* (2001).

The presence of a predominant direction allows the construction of a 1D finite element model along the pipe longitudinal axis; the unknown field is then approximated through the transversal cross-section by means of interpolation functions. This idea was exploited, initially, in structural mechanics by Carrera and Giunta (2010) by introducing Taylor (TE) polynomials as interpolation function. Subsequently, Lagrange (LE) and Legendre (HLE) functions were introduced, see Carrera and Petrolo (2012) and Pagani *et al.* (2016). The Carrera Unified Formulation (CUF), as presented in such works, allows to describe the unknown field as an arbitrary expansion of the generalized variables; in this way, the governing equations can be written in terms of *fundamental nuclei* (Carrera *et al.* (2014)), that are invariants of the approximation theory adopted. One-dimensional CUF capabilities were employed in many other areas of interest: composite beams, Giunta *et al.* (2013), aerospace and civil engineering structures, Carrera *et al.* (2012), Carrera and Pagani (2014), rotordynamics, Filippi and Carrera (2016) and multi-field analysis, Miglioretti and Carrera (2015), among the others. In recent works, CUF was extended to variable kinematics problems (Carrera and Zappino (2017)), in which a coupling between 3D and 1D models is exploited without affecting the formulation of the problem.

Preliminary results about the utilization of 1D TE CUF models for fluid-dynamics have been discussed by Varello (2013) and Pagani (2015). In the present work, one-dimensional flow models for incompressible and highly viscous fluids have been implemented employing the LE through the cross-section of the pipes. In this framework, it was possible an assessment of different models for the analysis of the flow in circular and non-circular conducts. The present paper is organized as follows: (1) first, CUF models for fluid-dynamics are presented; (2) then some numerical results are discussed and analyzed and (3) finally the key findings are drawn.
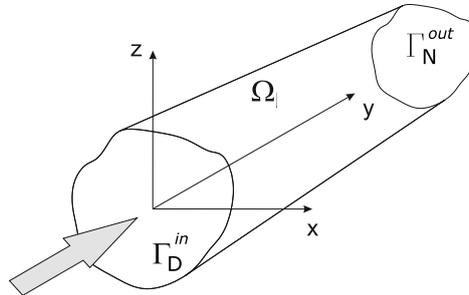
Fig. 1 Computational domain Ω

2. Stokes equations and Galerkin approximation

The domain, considered fixed, is assumed in a Cartesian coordinate system such as the one depicted in Fig. 1. Ω is usually referred to as computational domain or control volume. It is bounded, and its bounding surface is denoted by $\partial\Omega$, whereas Γ is used to refer to a generic surface in the domain. The outwardly oriented unit vector normal to the boundary $\partial\Omega$ is indicated with $\mathbf{n}$.

Let's consider the *Navier-Stokes* set of equations. In the complete form, they comprehend the conservation of mass, i.e. *continuity equation*, the conservation of *linear momentum* and the conservation of *energy*. These equations are based on the assumption that the fluid is a continuum not made of discrete particles, and the solution is not straightforward due to the presence of the non-linear convective term. However, there are some cases in which it is possible to neglect this contribute as in the case we are dealing with. Let the *Reynolds* number *Re* to be defined as follows

$$Re = \frac{|\mathbf{U}|\,\mathcal{D}}{\nu} \tag{1}$$

where $\mathcal{D}$ is a dimension representative of the domain Ω, $\mathbf{U}$ is the representative velocity and ν is the kinematic viscosity in $[m^2/s]$. Generally, in the case of highly viscous fluids, the Reynolds number can be small ($Re \ll 1$) and the contribution of the non-linear convective term can be neglected. In these cases, the Navier-Stokes set of equations for incompressible flow can be reduced to the so-called *Stokes equations*, which hold

$$\begin{cases} -\nu\Delta\mathbf{u} + \nabla p = \mathbf{f} & \text{in } \Omega \\ \nabla\cdot\mathbf{u} = 0 & \text{in } \Omega \\ \mathbf{u} = \mathbf{g^D} & \text{on } \Gamma_D \\ \nu\dfrac{\partial\mathbf{u}}{\partial\mathbf{n}} - p\,\mathbf{n} = \mathbf{t^N} & \text{on } \Gamma_N \end{cases} \tag{2}$$

where the first equation represents the momentum conservation while the second is the continuity equation. $\mathbf{u}$ represents the velocity in $[m/s]$, p is the pressure in $[m^2/s^2]$ and $\mathbf{f}$ is the vector of body forces acting in Ω. The last two equations represent the boundary conditions applied to the system; in particular, the first one describes a general non-homogeneous Dirichlet boundary condition at the *inlet* cross section while the second represents the Neumann boundary condition applied at the *outlet*

cross-section, see Fig. 1. It is remarked that, since we are taking into account a steady flow, all the derivatives in time are neglected.

The *weak* form of Stokes equations is formally obtained by taking the scalar product of the momentum equations with a vector function $\mathbf{v}$ (*test function*) belonging to a suitable functional space V (*test function space*), integrating over the computational domain Ω and applying the Green integration formula. Similarly, the continuity equation is multiplied by a *scalar test function q* belonging to a suitable *test functional space Q* and integrated over the computational domain Ω. The weak form of the momentum conservation for the Stokes problem, thus, read as follows

$$\int_{\Omega} \left[-\nu \, \Delta \mathbf{u} \cdot \mathbf{v} + \nabla p \cdot \mathbf{v} \right] \mathrm{d}\Omega = \int_{\Omega} \mathbf{f} \cdot \mathbf{v} \, \mathrm{d}\Omega \tag{3}$$

By using the Green formula for the Laplacian operator and for the divergence operator and considering ν constant for the fluid considered, Eq. (3) becomes

$$\int_{\Omega} \nu \, \nabla \mathbf{u} : \nabla \mathbf{v} \, \mathrm{d}\Omega - \int_{\Omega} p \, \nabla \cdot \mathbf{v} \, \mathrm{d}\Omega = \int_{\partial\Omega} \left(\nu \, \frac{\partial \mathbf{u}}{\partial \mathbf{n}} - p \, \mathbf{n} \right) \cdot \mathbf{v} \, \mathrm{d}\Gamma + \int_{\Omega} \mathbf{f} \cdot \mathbf{v} \, \mathrm{d}\Omega \tag{4}$$

$\forall \, \mathbf{v} \in V$. The term $\nabla \mathbf{u} : \nabla \mathbf{v}$ in Eq. (4) is

$$\nabla \mathbf{u} : \nabla \mathbf{v} = \mathrm{tr} \left(\nabla \mathbf{u}^T \, \nabla \mathbf{v} \right) \tag{5}$$

where the symbol tr stands for the trace of a square matrix. The mass conservation of the Stokes equation (second expression in Eq. (2)) is

$$-\int_{\Omega} q \, \nabla \cdot \mathbf{u} \, \mathrm{d}\Omega = 0 \tag{6}$$

$\forall \, q \in Q$. It should be noted that the negative sign in Eq. (6) has been included only for the sake of convenience.

2.1 Boundary conditions

In the case of mixed Dirichlet−Neumann homogeneous boundary conditions, Stokes problem can be significantly simplified. In fact, the integral term on the boundary $\partial\Omega$ in Eq. (4) can be expressed as a summation of two integrals over Γ_D and Γ_N. On the other hand, the test function space V is chosen in such a way that the test functions $\mathbf{v}$ vanish over Γ_D. It is therefore straightforward to demonstrate that, in the case of homogeneous boundary conditions,

$$\int_{\partial\Omega} \left(\nu \, \frac{\partial \mathbf{u}}{\partial \mathbf{n}} - p \, \mathbf{n} \right) \cdot \mathbf{v} \, \mathrm{d}\Gamma = 0 \tag{7}$$

Hence, the weak form of the Stokes problem with mixed Dirichlet−Neumann homogeneous boundary conditions in Eq. (2) is

Find $\mathbf{u} \in V = \left[\mathrm{H}^1_{\Gamma_D} (\Omega) \right]^3$, $p \in Q = \mathrm{L}^2 (\Omega)$ such that

$$\begin{cases} \displaystyle \int_{\Omega} \nu \, \nabla \mathbf{u} : \nabla \mathbf{v} \, \mathrm{d}\Omega - \int_{\Omega} p \, \nabla \cdot \mathbf{v} \, \mathrm{d}\Omega = \int_{\Omega} \mathbf{f} \cdot \mathbf{v} \, \mathrm{d}\Omega & \forall \, \mathbf{v} \in V \\[2ex] \displaystyle -\int_{\Omega} q \, \nabla \cdot \mathbf{u} \, \mathrm{d}\Omega = 0 & \forall \, q \in Q \end{cases} \tag{8}$$

where $L^2(\Omega)$ is the space of square-integrable functions on $\Omega \subset R$ and H^3 is the *Sobolev space* formed by the totality of functions $L^2(\Omega)$ such that all their derivatives up to order 3 belong to $L^2(\Omega)$.

2.2 Galerkin approximation

The Galerkin approximation of the Stokes problem with homogeneous boundary conditions as in Eq. (8) has the following form

Find $\mathbf{u}_h \in V_h$, $p_h \in Q_h$ such that

$$
\begin{cases}
\displaystyle \int_\Omega \nu \, \nabla \mathbf{u}_h : \nabla \mathbf{v}_h \, d\Omega - \int_\Omega p_h \, \nabla \cdot \mathbf{v}_h \, d\Omega = \int_\Omega \mathbf{f} \cdot \mathbf{v}_h \, d\Omega & \forall \, \mathbf{v}_h \in V_h \\[4mm]
\displaystyle - \int_\Omega q_h \, \nabla \cdot \mathbf{u}_h \, d\Omega = 0 & \forall \, q_h \in Q_h
\end{cases}
\tag{9}
$$

The terms u_h and p_h in Eqs. 9 are the discrete solutions of the Stokes problem in weak form (Eq. (8)). Let the bilinear forms $a : V \times V \to \mathbb{R}$ and $b : V \times Q \to \mathbb{R}$ to be defined as follows

$$
a(\mathbf{u}, \mathbf{v}) = \int_\Omega \nu \, \nabla \mathbf{u} : \nabla \mathbf{v} \, d\Omega
\tag{10}
$$

$$
b(\mathbf{u}, q) = -\int_\Omega q \, \nabla \cdot \mathbf{u} \, d\Omega
\tag{11}
$$

With this notation, the Galerkin approximation of the Stokes equation reads

Find $\mathbf{u}_h \in V_h$, $p_h \in Q_h$ such that

$$
\begin{cases}
a(\mathbf{u}_h, \mathbf{v}_h) + b(\mathbf{v}_h, p_h) = (\mathbf{f}, \mathbf{v}_h) & \forall \, \mathbf{v}_h \in V_h \\[2mm]
b(\mathbf{u}_h, q_h) = 0 & \forall \, q_h \in Q_h
\end{cases}
\tag{12}
$$

where $V_h \subset V$ and $Q_h \subset Q$ represent two families of finite dimensional subspaces depending on a real positive discretization parameter h.

3. One-dimensional CUF models for Stokes flow

Several types of flows in nature can be considered as mono-dimensional, and then can be approximated via 1D models. Nevertheless, simplified models are not able to describe higher-order phenomena and refined models may be necessary. The one-dimensional Carrera Unified Formulation (CUF) is here used along with FEM to approximate the Galerkin formulation of the Stokes equations.

According to CUF, the velocity field $\mathbf{u}_h$ and the pressure field p_h are expressed, in a unified manner, as a generic expansion of the generalized unknowns through arbitrary functions of the cross-section domain coordinates

$$
\mathbf{u}_h(x, y, z) = F_\tau^U(x, z)\mathbf{u}_\tau(y), \qquad\qquad \tau = 1, 2, \cdots, M^U
\tag{13}
$$

$$
p_h(x, y, z) = F_m^P(x, z)p_m(y), \qquad\qquad m = 1, 2, \cdots, M^P
\tag{14}
$$

where $\mathbf{u}_\tau(y)$ is the vector of velocity components and $p_m(y)$ is the scalar pressure, function of the pipe axis y. According to CUF, τ and m indicate summations. F_τ^U or F_m^P correspond to the expanding functions on the cross-section Γ, which is defined in the Cartesian plane xz, and M^U and M^P are the number of terms in the expansion, for velocity and pressure respectively. These terms are strictly connected with the expansion order adopted in the description of the velocity and pressure fields, and, indeed, with the accuracy of the model. A brief introduction of the cross-sectional functions that have been adopted in the past few years in the framework of the CUF is presented in the following sections.

3.1 Taylor expansions

Taylor expansion models (TE) employ hierarchical sets of 2D polynomials from Maclaurin series of the type $x^i z^j$ for the definition of $F_\tau(x, z)$. In this work the polynomial approximation order for velocity and pressure are denoted to as N^U and N^P, respectively. For instance, a second order model, for the approximation of the velocity field ($N^U{=}2$), makes use of constant, linear and quadratic expansion terms

$$u_x(x, y, z) = u_{x_1}(y) + x\, u_{x_2}(y) + z\, u_{x_3}(y) + x^2\, u_{x_4}(y) + xz\, u_{x_5}(y) + z^2\, u_{x_6}(y)$$

$$u_y(x, y, z) = u_{y_1}(y) + x\, u_{y_2}(y) + z\, u_{y_3}(y) + x^2\, u_{y_4}(y) + xz\, u_{y_5}(y) + z^2\, u_{y_6}(y) \qquad (15)$$

$$u_z(x, y, z) = u_{z_1}(y) + x\, u_{z_2}(y) + z\, u_{z_3}(y) + x^2\, u_{z_4}(y) + xz\, u_{z_5}(y) + z^2\, u_{z_6}(y)$$

where $u_{x_1}, u_{x_2} \cdots, u_{z_6}$ are the primary variables. The same methodology is valid for the expansion of the scalar pressure. In this context, it is possible to increase the polynomial order with ease by adding higher-order terms to the unknown, enhancing the accuracy of the approximation. TE models have been extensively studied in many works, see for example Carrera *et al.* (2014), Giunta *et al.* (2013).

3.2 Lagrange expansions

Lagrange expansion models (LE) are based on the use of Lagrange-type polynomials as generic expansions on the pipe cross-section. The transversal physical surface is subdivided into a number of local expansion sub-domains, whose polynomial degree depends on the type of Lagrange expansion employed. Three-node linear L3, four-node bilinear L4, nine-node quadratic L9, and sixteen-node cubic L16 polynomials have been employed in the framework of CUF. As an example, the L9 quadratic model holds the following approximation of the velocity field

$$u_x(x, y, z) = F_1\, u_{x_1}(y) + F_2\, u_{x_2}(y) + F_3\, u_{x_3}(y) + \cdots + F_9\, u_{x_9}(y)$$

$$u_y(x, y, z) = F_1\, u_{y_1}(y) + F_2\, u_{y_2}(y) + F_3\, u_{y_3}(y) + \cdots + F_9\, u_{y_9}(y) \qquad (16)$$

$$u_z(x, y, z) = F_1\, u_{z_1}(y) + F_2\, u_{z_2}(y) + F_3\, u_{z_3}(y) + \cdots + F_9\, u_{z_9}(y)$$

The main feature of LE models is the possibility to make use of local expansions of pure unknowns variables, being these arbitrarily placed over the cross-section surface. In this case, $F_1, \cdots, F_9$ are

the following quadratic Lagrange polynomials

$$F_\tau = \tfrac{1}{4}(r^2 + r\, r_\tau)(s^2 + s\, s_\tau), \qquad \tau = 1, 3, 5, 7$$

$$F_\tau = \tfrac{1}{2}s_\tau^2(s^2 + s\, s_\tau)(1 - r^2) + \tfrac{1}{2}r_\tau^2(r^2 + r\, r_\tau)(1 - s^2), \qquad \tau = 2, 4, 6, 8 \qquad (17)$$

$$F_\tau = (1 - r^2)(1 - s^2), \qquad \tau = 9$$

where r and s vary above the cross-sectional natural plane between -1 and $+1$, and r_τ and s_τ represent the locations of the roots of the nine-node Lagrange polynomial set. According to LE modelling, higher-order theories can be opportunely formulated by increasing the polynomial order (e.g., cubic L16) or by using a combination of polynomial sets on the conduit cross-section to have a piece-wise refined velocity (or pressure) field (see Carrera and Petrolo (2012)).

4. Finite element formulation

The main advantage of CUF is that it allows to write the governing equations in a unified manner. The class of expanding functions (e.g., TE, LE) and the polynomial order of the theory become arbitrary inputs of the model. In the case of FE approximation of the pipe axis, the generalized velocities $\mathbf{u}_\tau(y)$ and pressures $p_m(y)$ are described as a function of the unknown nodal vectors, $\mathbf{u}_{\tau i}$ and p_{mt}, and the 1D shape functions, N_i and N_t, as follows

$$\mathbf{u}_\tau(y) = N_i^U(y)\, \mathbf{u}_{\tau i}, \qquad i = 1, \ldots, p^U + 1 \qquad (18)$$

$$p_m(y) = N_t^P(y)\, p_{mt}, \qquad i = 1, \ldots, p^P + 1 \qquad (19)$$

where i and t stand for summation. p^U and p^P represent the order of the FEM shape functions for velocity and pressure, respectively. The shape functions N_i^U and N_t^P can be arbitrary and, in general, different; in this work the classic Lagrangian 1D shape functions are considered, in particular, two-node linear (B2), three-node quadratic (B3) and four-nodes cubic (B4) are employed, (see Zienkiewicz *et al.* (1977)).

Combining the FE approximation in Eqs. (18) and (19) with CUF (Eqs. (14)) the final expressions describing the unknown fields are

$$\mathbf{u}_h(x, y, z) = F_\tau^U(x, z)\, N_i^U(y)\, \mathbf{u}_{\tau i}, \qquad \tau = 1, \ldots, M^U \quad i = 1, \ldots, p^U + 1 \qquad (20)$$

$$p_h(x, y, z) = F_m^P(x, z)\, N_t^P(y)\, p_{mt}, \qquad m = 1, \ldots, M^P \quad t = 1, \ldots, p^P + 1 \qquad (21)$$

4.1 CFD fundamental nuclei

According to 1D CUF, the generic discrete test functions $\mathbf{v}_h \in V_h$ and $q_h \in Q_h$ are approximated in a manner equivalent to Eqs. (20) and (21). It is sufficient, therefore, that the Galerkin approximation in Eq. (9) is verified for each function of the basis of V_h and Q_h, because all the functions in the spaces V_h and Q_h are a linear combination of the basis functions (see Quarteroni (2009), Brezzi (1974)). Hence, the solution of the Galerkin approximation in the framework of CUF comes from
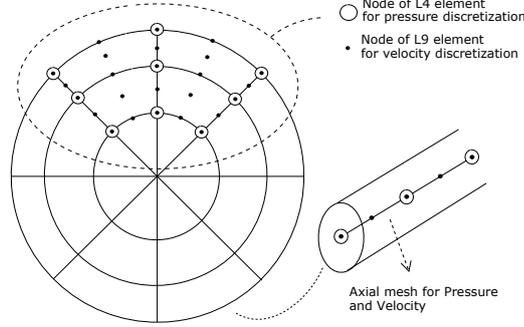
Fig. 2 CUF LE model discretizations of pressure and velocity fields

the following system of equations

Find $\mathbf{u}_h \in V_h$, $p_h \in Q_h$ such that

$$\begin{cases} a\left(\mathbf{u}_h, \boldsymbol{\varphi}_{\tau i e}\right) + b\left(\boldsymbol{\varphi}_{\tau i e}, p_h\right) = \left(\mathbf{f}, \boldsymbol{\varphi}_{\tau i e}\right) & \forall \tau, \ \forall i, \ \forall e \\ b\left(\mathbf{u}_h, \phi_{mt}\right) = 0 & \forall m, \ \forall t \end{cases} \quad (22)$$

with $\tau = 1, \ldots, M^U$, $i = 1, \ldots, p^U + 1$, $e = 1, \ldots, 3$, $m = 1, \ldots, M^P$, $t = 1, \ldots, p^P + 1$. The index e refers to the three components of the velocity field, and

$$\boldsymbol{\varphi}_{\tau i e}\left(x, y, z\right) = \left\{ \begin{array}{l} \delta_{1e}\, F_\tau^U\left(x, z\right) N_i^U\left(y\right) \\ \delta_{2e}\, F_\tau^U\left(x, z\right) N_i^U\left(y\right) \\ \delta_{3e}\, F_\tau^U\left(x, z\right) N_i^U\left(y\right) \end{array} \right\} \quad (23)$$

are the bases of the space V_h due to the 1D CUF approximation and $\delta_{\mathsf{k}e} = 1$ if $e = \mathsf{k}$, 0 otherwise. Similarly,

$$\phi_{mt}\left(x, y, z\right) = F_m^P\left(x, z\right) N_t^P\left(y\right) \quad (24)$$

For the sake of clarity, indices s (instead of τ) and j (instead of i) are introduced into Eq. (22) for the CUF approximation of the discrete solution $\mathbf{u}_h$ (see Eq. (20)). After extensive mathematical manipulations (see Varello (2013)), Eq. (22) becomes the following system of algebraic equations

$$\begin{cases} \mathbf{A}^{\tau s i j}\, \mathbf{q}_{sj} + \mathbf{B}^{\tau m i t^T} p_{mt} = \mathbf{F}^{\tau i} & \forall \tau, \ \forall i \\ \mathbf{B}^{m s t j}\, \mathbf{q}_{sj} = \mathbf{0} & \forall m, \ \forall t \end{cases} \quad (25)$$

where $\mathbf{A}^{\tau s i j}$ is the *fundamental nucleus* related to the bilinear form $a\left(\mathbf{u}_h, \boldsymbol{\varphi}_{\tau i e}\right)$ of the 1D CUF model

$$\mathbf{A}^{\tau s i j} = \left[\nu \int_L N_i^U N_j^U \, \mathrm{d}y \int_{\Gamma_S} F_{\tau,x}^U F_{s,x}^U \, \mathrm{d}\Gamma + \nu \int_L N_{i,y}^U N_{j,y}^U \, \mathrm{d}y \int_{\Gamma_S} F_\tau^U F_s^U \, \mathrm{d}\Gamma + \right.$$
$$\left. \nu \int_L N_i^U N_j^U \, \mathrm{d}y \int_{\Gamma_S} F_{\tau,z}^U F_{s,z}^U \, \mathrm{d}\Gamma \right] \mathbf{I} \quad (26)$$
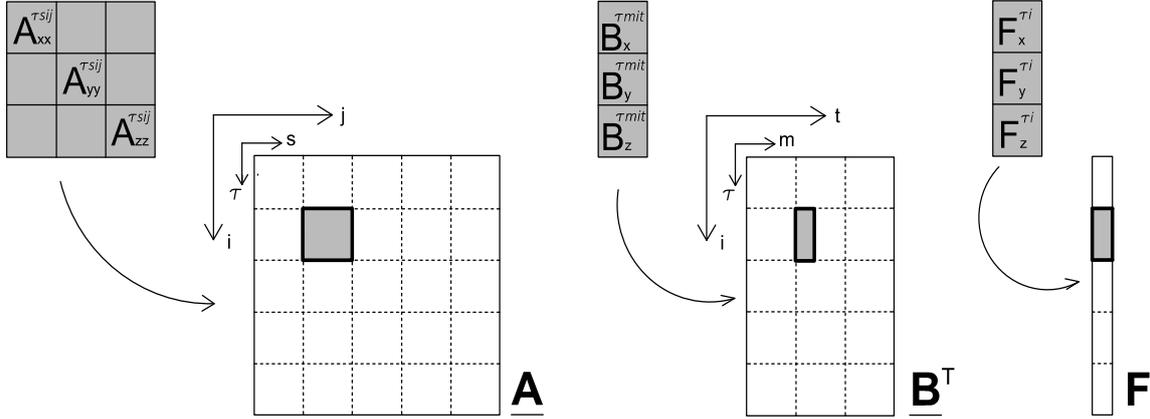
Fig. 3 Procedure to build the finite element matrices and vectors expanding the fundamental nuclei. Scheme for *momentum* conservation equation

$\mathbf{B}^{\tau m i t\, T}$ is the *fundamental nucleus* related to the bilinear form $b\left(\boldsymbol{\varphi}_{\tau i e}, p_h\right)$

$$\mathbf{B}^{\tau m i t\, T} = \left\{ \begin{array}{c} -\displaystyle\int_L N_i^U\, N_t^P\, \mathrm{d}y \int_{\Gamma_S} F_{\tau,x}^U\, F_m^P\, \mathrm{d}\Gamma \\[2ex] -\displaystyle\int_L N_{i,y}^U\, N_t^P\, \mathrm{d}y \int_{\Gamma_S} F_\tau^U\, F_m^P\, \mathrm{d}\Gamma \\[2ex] -\displaystyle\int_L N_i^U\, N_t^P\, \mathrm{d}y \int_{\Gamma_S} F_{\tau,z}^U\, F_m^P\, \mathrm{d}\Gamma \end{array} \right\} \tag{27}$$

$\mathbf{B}^{m s t j}$ is the *fundamental nucleus* corrisponding to the bilinear form $b\left(\mathbf{u}_h, \phi_{mt}\right)$

$$\mathbf{B}^{m s t j} = \left\{ \begin{array}{c} -\displaystyle\int_L N_t^P\, N_j^U\, \mathrm{d}y \int_{\Gamma_S} F_m^P\, F_{s,x}^U\, \mathrm{d}\Gamma \\[2ex] -\displaystyle\int_L N_t^P\, N_{j,y}^U\, \mathrm{d}y \int_{\Gamma_S} F_m^P\, F_s^U\, \mathrm{d}\Gamma \\[2ex] -\displaystyle\int_L N_t^P\, N_j^U\, \mathrm{d}y \int_{\Gamma_S} F_m^P\, F_{s,z}^U\, \mathrm{d}\Gamma \end{array} \right\}^T \tag{28}$$

and $\mathbf{F}^{\tau i}$ is the *fundamental nucleus* related to the term $\left(\mathbf{f}, \boldsymbol{\varphi}_{\tau i e}\right)$.

$$\mathbf{F}^{\tau i} = \int_\Omega F_\tau^U\, N_i^U\, \mathbf{f}\, \mathrm{d}\Omega \tag{29}$$
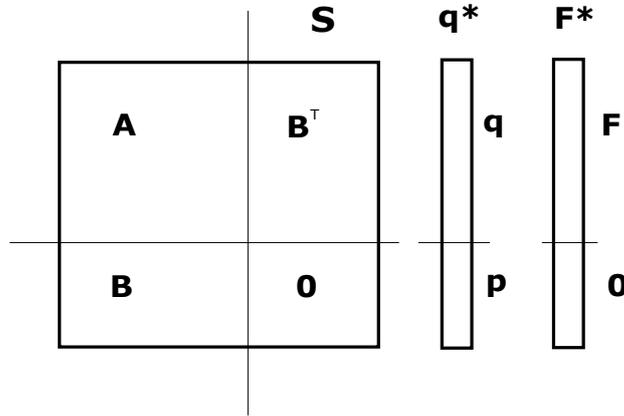
Fig. 4 Condensed problem in FE scheme

In Eq. (26), $\mathbf{I}$ is the 3×3 identity matrix.

Like in other applications of CUF, the mathematical expressions of the nuclei are formally independent of the theory orders (N^U and N^P) and on the FEM shape functions (p^U and p^P). These nuclei have to be expanded against the indices τ, s, m, i, j, and t. For further details on the expansions of the fundamental nuclei, interested readers are referred to Carrera *et al.* (2014), where mechanical problems are mainly addressed. This expansion leads to the construction of the elemental FE arrays associated to the Galerkin approximation of the Stokes problem. The expansion is carried out by following a scheme depicted in Fig. 3. Assembling all the finite elements, the final system of equations is formulated as

$$\begin{cases} \mathbf{A}\,\mathbf{q} \,+\, \mathbf{B}^T\mathbf{p} \,=\, \mathbf{F} \\ \mathbf{B}\,\mathbf{q} \,=\, \mathbf{0} \end{cases} \tag{30}$$

It is interesting to note the following relation between the nuclei of the matrices $\mathbf{B}^T$ and $\mathbf{B}$

$$\mathbf{B}^{mstj\,T} \,=\, \mathbf{B}^{\tau mit} \tag{31}$$

which is formally true aside from the use of different indices.

The system of Eq. (30) can be written collecting matrices $\mathbf{A}$, $\mathbf{B^T}$, $\mathbf{B}$ and a zero matrix $\mathbf{0}$ in a single symmetrical matrix $\mathbf{S}$, collecting the unknowns $\mathbf{q}$ and $\mathbf{p}$ in a single vector of unknowns $\mathbf{q}^\star$, and collecting the column vectors $\mathbf{F}$ and $\mathbf{0}$ in a single column vector $\mathbf{F}^\star$ following the scheme in Fig. 4.

$$\mathbf{S}\mathbf{q}^\star \,=\, \mathbf{F}^\star \tag{32}$$

interested readers can find more detailes about the imposition of the boundary conditions in Ref. Varello (2013)

5. Numerical results

The one-dimensional CUF for fluid-dynamics is assessed in this section. A number of refined models are compared with analytical solutions, whenever possible, or with finite volume results obtained with commercial software tool. The first case study consists in the evaluation of fluid parameters in the case of Poiseuille flow in a cylindrical pipe. The second numerical assessment confirms the validity of the technique in presence of different boundary conditions, whereas the third subsection deals with the study of Stokes flow in a square-section cylindrical pipe.

The length of the pipe considered is $L = 6$ m and the radius is $r = 1$ m in the case of the circular section. In case of square cross-section, the side is $s = 2$ m. All the subsequent analyses present a homogeneous Dirichlet boundary condition on the lateral surface Γ_D^{Lat} (no-slip condition), and a homogeneous Neumann boundary condition on the outlet section Γ_N^{Out}. Conversely, the inlet section Γ_D^{In} presents, according to each case study considered, different nonhomogeneous Dirichlet boundary conditions. No body forces are applied to the fluid and thus **f = 0** is taken into account in the Stokes equations. The fluid has a viscosity ν equal to $10^{-2} m^2/s$ satisfying the condition of $Re \ll 1$ for the velocity profiles introduced afterwards. If not differently specified, CUF models are discretized with 10 1D FEM elements, which ensure convergent results.

5.1 Poiseuille flow in circular-section pipe

The first case analyzed is the Poiseuille flow in the cylindrical pipe considered. The Poiseuille flow is the condition achieved by a flow in cylindrical pipe when the Reynolds number is very small. For this kind of flows, the analytical solution exists and, represents a good benchmark to assess the 1D CUF theory for fluid-dynamics.

In the Poiseuille flow, the velocity **u** does not vary along the longitudinal axis y. In particular, the axial velocity component u_y describes a paraboloid in which the maximum value $u_{y_{max}}$ occurs at the centre of the section. To simulate this kind of flow, the following non-homogeneous Dirichlet boundary condition is given at the inlet section Γ_D^{in}

$$\begin{cases} u_x = 0 \\ u_y = 10^{-4} \left(1 - x^2 - z^2\right) \qquad \text{on } \Gamma_D^{in} \\ u_z = 0 \end{cases} \tag{33}$$

According to the Poiseuille analytic solution Stera and Salak (1993), the paraboloidal inlet velocity profile, which is depicted in Fig. 5, should remain constant over the pipe axis. As shown in Fig. 5, which gives the Poiseuille profiles for different 1D models and reference solution, a second-order for velocity and a zero-order for pressure are sufficient to detect the exact solution in the case of TE. On the contrary, in the case of LE, 5 cubic cross-section subdomains for velocity and 5 quadratic polynomials for the pressure are necessary to find the solution with a good approximation, as resumed in Table 1. The finite volume solutions are obtained by (OpenFoam OpenFOAM Foundation (2011)) and they come from three different discretizations. Namely, the model $OpenFOAM_A$ was constructed with 2640 finite volumes (132x20 mesh, where 132 stands for the number of volumes on the cross-section and 20 is the discretization along the y-axis), $OpenFOAM_B$ has 13600 (340 x 40) finite volumes, and $OpenFOAM_C$ has 108800 (1368 x 80) finite volumes. The value of pressure decreases linearly along the pipe and does not have any dependency on the x and z coordinates. In

Table 1 Inlet pressure and maximum axial velocity at y=3 in terms of percentage errors versus analytical solution for the Poiseuille flow. Comparison of OpenFOAM results with CUF results

Model	$e_p(\%)$	$e_{u_y}(\%)$	$DOFs$
OpenFOAM			
OpenFOAM$_A$	-0.72	-2.56	10560
OpenFOAM$_B$	-0.25	-0.97	54400
OpenFOAM$_C$	0.21	-0.39	435520
CUF - TE			
N^U2, N^P0	-0.05	-0.05	389
CUF - LE			
$5L9^U, 5L4^P$	+1.83	-2.19	2493
$5L16^U, 5L9^P$	-0.03	+0.24	5361

particular, it is important to underline that the outlet value is equal to zero, exactly as described by the Poiseuille analytical solution, see Fig. 6. Linear to cubic shape functions (i.e., B3 and B4) were used for the FE discretization along the y axis. The choice of the class of expansion is a key point of the analysis due to instability; in fact, finite elements of the same polynomial degree for both velocity and pressure are in general unstable, giving rise to typical spurious pressure modes. For the sake of completeness, a convergence analysis is provided; in particular, an investigation on the L^2 norm of relative error was performed. The convergence was first compared between TE and LE models, by varying the order of expansion over the section, see Fig. 7(a) . Then, as presented in Fig. 7(b), two specific LE models were considered, and the relative error by varying the FE meshes along the longitudinal axis was evaluated. As Fig. 7(a) suggests, in the case of Poiseuille flow in circular pipes, the TE models are able to detect the correct solution without increasing the order of expansion, in contrast with LE ones. Regarding Fig. 7(b), a stability problem, and a consequent increasing of the
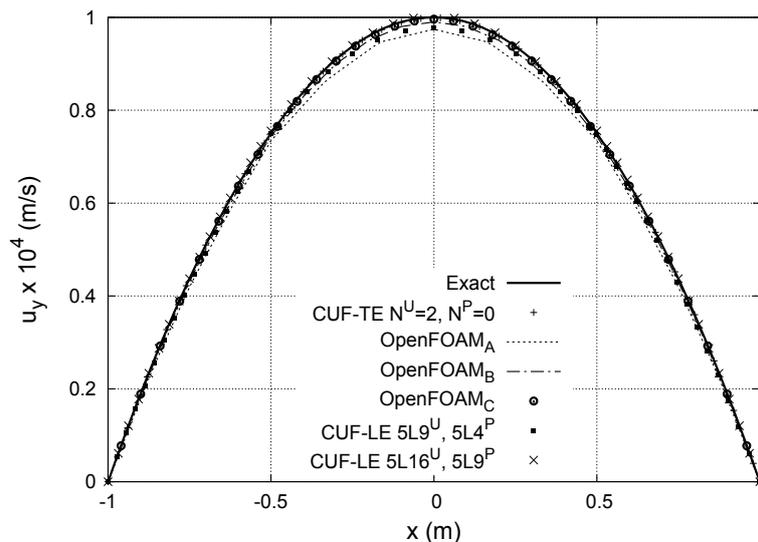

Fig. 5 Poiseuille flow velocity profile at $y = 3$ m, $z = 0$

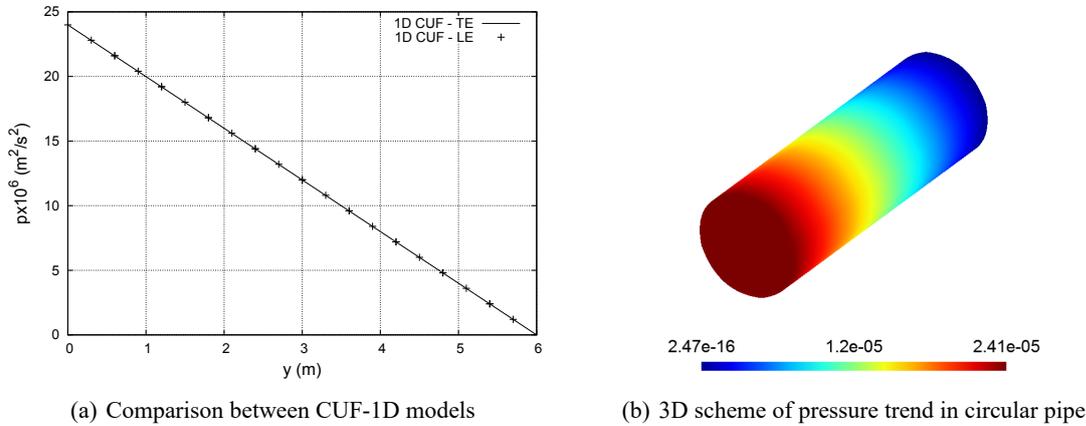(a) Comparison between CUF-1D models (b) 3D scheme of pressure trend in circular pipe

Fig. 6 Pressure trend comparison between LE and TE models along the longitudinal axis y (a), 3D scheme of the pressure trend of the Lagrange model $5L16^U$ - $5L9^P$, results are in m^2/s^2 (b). Poiseuille flow

error, is evident whenever the 1D elements for FE discretization of the y axis are the same for both the pressure and velocity.

5.2 Fourth-order and fifth-order inlet velocity profiles in circular pipes

The Poiseuille flow has been used to assess the 1D CUF models for Stokes fluid-dynamics; it is the most simple flow in a pipe, and the condition of a constant pressure over the section is commonly used by classical one-dimensional models for fluid-dynamics. In this section, the capabilities of the 1D CUF models are presented in the description of more complex flow. Thus, fourth-order and fifth-order velocity profiles are hereinafter introduced at the inlet cross-section and the results from 1D CUF models are compared with those obtained via OpenFoam. As first case, the following fourth-

(a) Convergence analysis of TE and LE models (b) Convergence analysis of two specific LE models
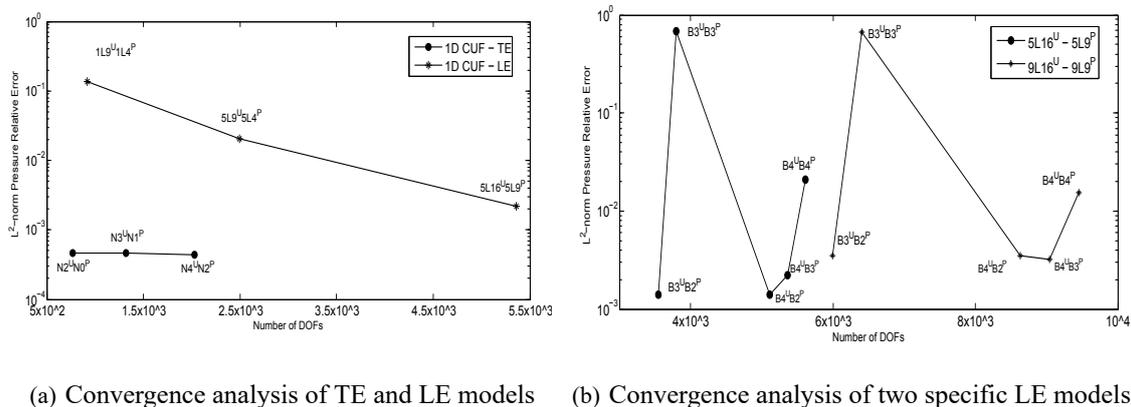
Fig. 7 Trend of L^2 norm of pressure relative error. Convergence analysis of TE and LE models (a) and of two different Lagrange models (b)

Table 2 Maximum inlet pressure and maximum axial velocity at $y = 3$m. Comparison of OpenFOAM results with CUF results, fourth-order inlet velocity profile

Model		$p \times 10^5 (m^2/s^2)$	$u_y \times 10^5 (m/s)$	$DOFs$
		OpenFOAM		
OpenFOAM$_A$		1.70	6.50	10560
OpenFOAM$_B$		1.79	6.53	54400
OpenFOAM$_C$		1.87	6.36	435520
		CUF-TE		
N^U	N^P			
8	7	1.86	6.66	6651
8	6	1.86	6.66	6403
6	5	1.86	6.66	4095
6	4	1.86	6.66	3909
4	3	1.79	6.66	2155
4	2	1.79	6.66	2031
		CUF-LE		
$5L9^U$	$5L4^P$	1.75	6.53	2493
$5L16^U$	$5L9^P$	1.82	6.67	5361
$9L16^U$	$9L9^P$	1.84	6.66	9045

order velocity profile is enforced at the inlet cross-section Γ_D^{in}

$$\begin{cases} u_x = 0 \\ u_y = 10^{-4} \left(1 - x^2 - z^2\right)^2 \qquad \text{on } \Gamma_D^{in} \\ u_z = 0 \end{cases} \tag{34}$$

Note that the flow is still axisymmetric and that the other boundary conditions remain the same as in the previous section. According to the considerations done before, the longitudinal mesh is kept different between velocity and pressure: 10 cubic B4 Lagrange elements for velocity and 10 quadratic B3 for pressure are employed.

Table 2 shows the maximum value of the pressure at the inlet and the maximum value of the axial velocity in the middle of the pipe. TE model with N^U=6 and N^P=4 provides convergent results, whereas LE model needs 9 cubic elements for velocity and 9 quadratic ones for pressure. It is clear from Table 2 that both one-dimensional models, TE and LE, can approach the finite volume solution with a drastic reduction of degrees of freedom.

In the case of the fourth-order velocity inlet profile, u_y is still axisymmetric, but, it changes along the longitudinal axis y, as depicted in Fig. 8(a). In particular, the velocity presents a *transition* area in which the profile moves from a 4th-order to a 2nd-order Poiseuille flow. The behaviour of the pressure across the section is drawn in Fig. 8(b). Due to the inlet boundary condition, also the pressure trend presents a variation along the longitudinal axis; as expected, the pressure has an axisymmetric behaviour at the beginning of the pipe, and then tends to become constant over the section, approximately at $1/10$ of the length of the cylinder.

As the fifth-order inlet velocity profile concerns, it is not axisymmetric. It means that the following
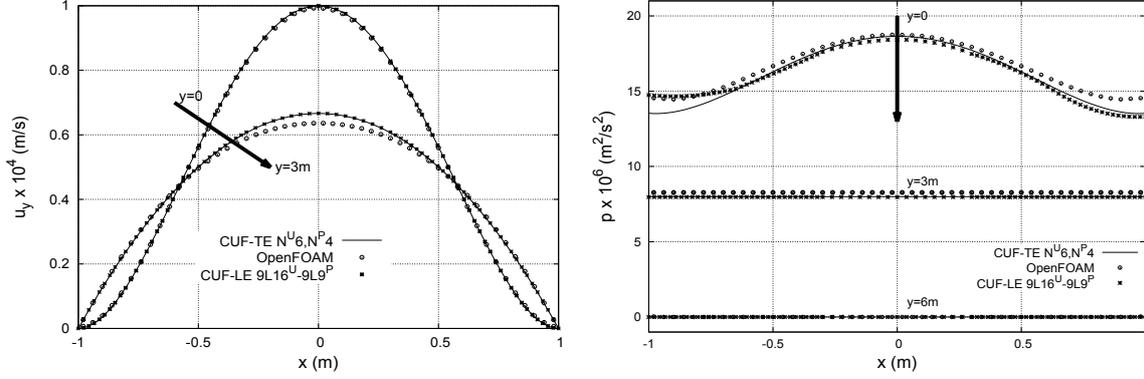
(a) Axial velocity variation over the different sections

(b) Pressure variations over the different sections

Fig. 8 Fourth-order inlet boundary condition. The profile for axial velocity u_y (a), and for pressure (b). Comparison of OpenFOAM results with CUF reuslts

Dirichlet non-homogeneous boundary condition was imposed on the first section of the pipe

$$\begin{cases} u_x = 0 \\ u_y = 10^{-4}\left(1 - x^2 - z^2\right)\left(1/4 + xz + x^3\right) \qquad \text{on } \Gamma_D^{\text{in}} \\ u_z = 0 \end{cases} \qquad (35)$$

The meshes along the y-axis remain unvaried, as well as the other boundary conditions. As a consequence, the flow obtained through the first sections is no more axisymmetric and it is requested a higher-order expansion, as it is possible to verify in Table 3, which gives the maximum inlet pressure value and maximum axial velocity at mid-span. The axial velocity profiles at various cross-sections till the mid-span (where the flow is fully developed) are depicted in Fig. 9. In this case the transition area is longer than the previous one faced for the fourth-order profile, as drown in Fig. 10. Nonetheless, the behaviour of velocity u_y gradually tends to the more natural condition of axial-symmetry, due to the outlet and lateral boundary conditions.

As expected, the pressure is not constant across the sections at the beginning of the pipe; it approaches gradually the constant profile typical of Poiseuille flow. First it becomes flat, then decreases linearly up to the outlet.

The following comments arise from these analyses:

- The different orders of velocity inlet profile represent an important assessment for the 1D CUF theory for fluid-mechanics due to its capability to predict the evolution of complex flows also when they are not axisymmetric.

- In the case of high-order flows, as suggested by Tables 2 and 3, appropriate accuracy of LE would require more DOFs than comparable TE models for the considered analysis cases.

- As it is possible to verify in the Table 3, one-dimensional models allow for detecting the solution with a drastic reduction of the computational efforts, compared to finite volume solutions.

Table 3 Maximum inlet pressure and maximum axial velocity at $y = 3$m. Comparison of OpenFOAM results with CUF results, fifth-order inlet velocity profile

Model		$p \times 10^6 (m^2/s^2)$	$u_y \times 10^5 (m/s)$	$DOFs$
		OpenFOAM		
OpenFOAM$_A$		7.20	2.43	10560
OpenFOAM$_B$		8.17	2.44	54400
OpenFOAM$_C$		9.08	2.35	435520
		CUF-TE		
N^U	N^P			
10	9	9.52	2.50	9823
8	7	9.48	2.50	6651
8	6	9.57	2.50	6403
6	5	9.23	2.50	4095
6	4	10.72	2.50	3909
5	4	10.80	2.50	3048
		CUF-LE		
$9L16^U$	$9L9^P$	9.19	2.50	9045
$20L16^U$	$20L9^P$	9.36	2.50	19818

5.3 Second-order flow in square-section pipe

The last numerical assessment of this paper aims at demonstrating the capabilities of LE CUF models to deal with complex and unconventional computational domains with ease. In particular, the flow through a square-section pipe have been evaluated, using LE one-dimensional models. The flow considered keeps the viscosity of the previous cases as well as the boundary conditions on the outlet and lateral surfaces. At the inlet section, a second-order velocity profile is enforced, the same used for the Poiseuille flow in the cylindrical pipe.

As in other fluid-dynamics problems, velocity and pressure fields are described by different order
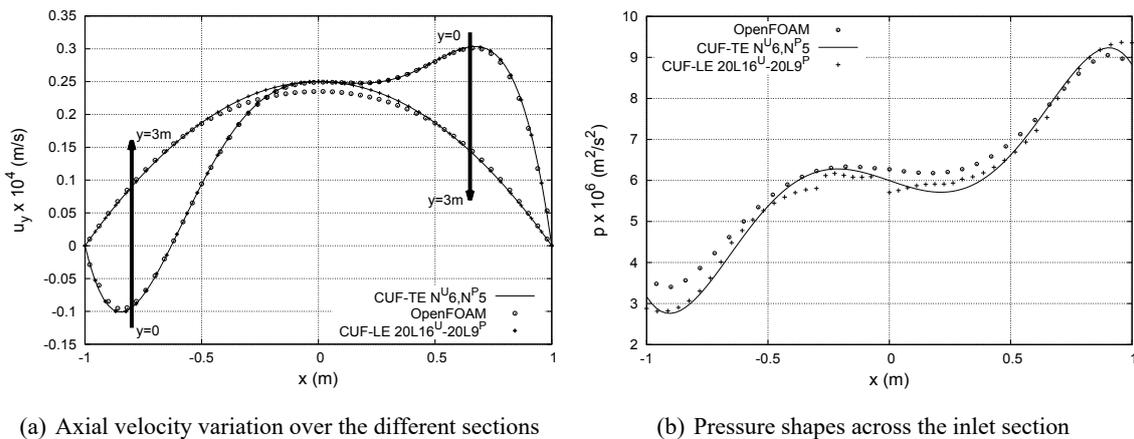

(a) Axial velocity variation over the different sections

(b) Pressure shapes across the inlet section

Fig. 9 Fifth-order inlet boundary condition. Transition of u_y axial velocity (a) pressure shapes across the inlet section (b) Comparison of OpenFOAM results with CUF results
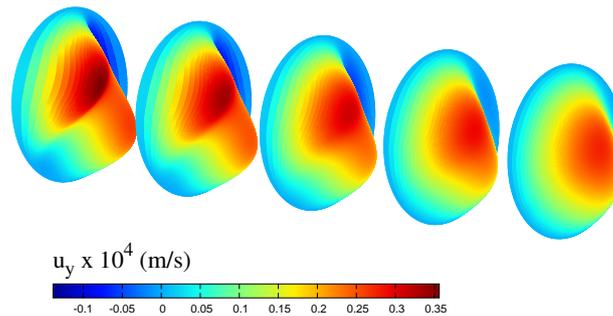
u_y x 10^4 (m/s)

Fig. 10 3D plot of axial velocity profile through the transition area in [m/s]. Fifth-order inlet boundary condition, TE model, $N^U = 6, N^P = 5$

polynomials; commonly, the pressure order is smaller than the velocity one, as shown in Fig. 11, which gives an example of LE modelling for the case under consideration. The first analysis consists of a comparison among schemes with different polynomial orders. Subsequently, some results about using the same order for pressure and velocity are presented. According to Fig. 12(a), in which the axial component of velocity u_y is depicted, some aspects about the order of polynomials and the boundary effects are relevant. In fact, the case $1L16^U$ is not able to detect the maximum value of 10^{-4} imposed, probably due to its cubic nature. At the same time, the $1L9^U$ case can find the maximum imposed, but does not perceive the decrease of axial velocity detected by the $4L9^U$ model. This question is evident in Fig. 13(a), (b), (c), where u_y is drawn on yz plane. According to this figure, the model with 4 Lagrange sub-domains is the only one presenting a decrease between inlet and midspan sections. As seen for the velocity, the pressure response depicted in Fig. 12(b) is affected by the boundary effects close to the inlet cross-section; nevertheless, each model presents a uniform decay along the conduct. While the order chosen for the velocity does not affect considerably the results, this is not true for the pressure field. For this reason, it is important to underline the necessity of keeping the pressure order smaller than the velocity one. When this condition is not satisfied, one can observe some stability problems concerning the pressure trend, see Fig. 14. As suggested by this figure, the choice of the expansion order across the section (Fig. 14(b)) and, of course, along the longitudinal axis (Fig. 14(a)), is an important parameter in fluid-dynamic analyses.

Due to this last section, we can confirm 1D CUF as an efficient and alternative tool for computational fluid-dynamics also in case of the non-circular section. This formulation allows to impose
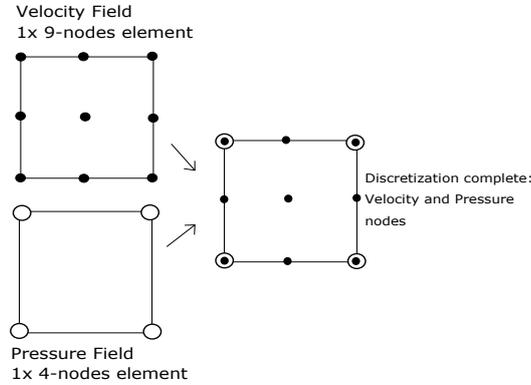
Fig. 11 Example of Lagrange elements across the section. 1xL9 for Velocity and 1xL4 for Pressure

different velocity profile with ease, and offers a simple way to manage the boundary.

6. Conclusions

In this work, CUF has been used for the analysis of incompressible, laminar and viscous fluids in rigid pipes. In particular, some higher-order 1D models for Stokes flows have been proposed. According to CUF, the primary variables of the flow (i.e. velocity and pressure) are expressed as arbitrary expansion of the generalized unknowns. By using these expanding functions on the cross-sectional plane, a unified finite element method has been developed straightforwardly. The case of Poiseuille flow has been taken into account as numerical assessment, and then more complex flows have been analyzed. In particular, Taylor expansion (TE) and Lagrange (LE) 1D models have been
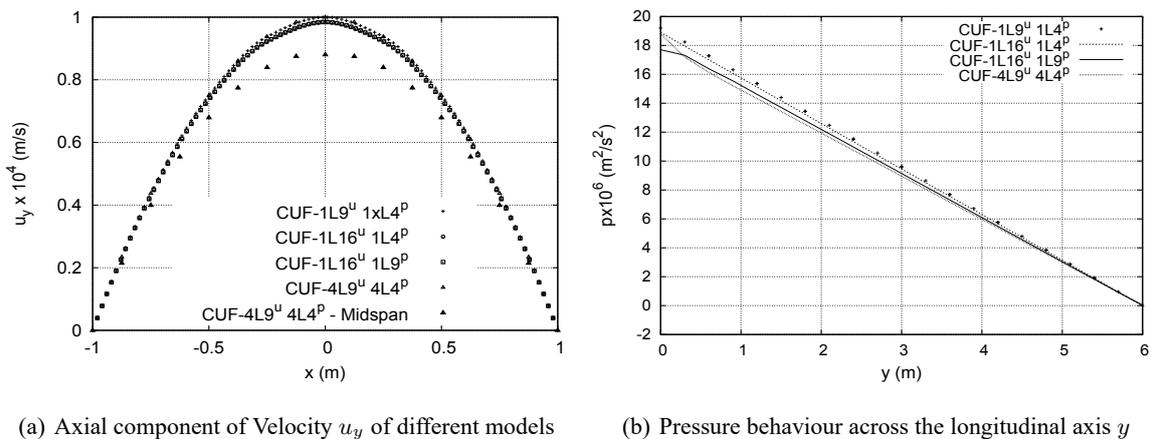

(a) Axial component of Velocity u_y of different models

(b) Pressure behaviour across the longitudinal axis y

Fig. 12 Second-order flow in a square-section pipe. (a) Parabolic behaviour of the axial velocity (b) decreasing pressure along the conduct

(a) $1L9^U$ - $1L4^P$

(b) $1L16^U$ - $1L4^P$

(c) $4L9^U$ - $4L4^P$

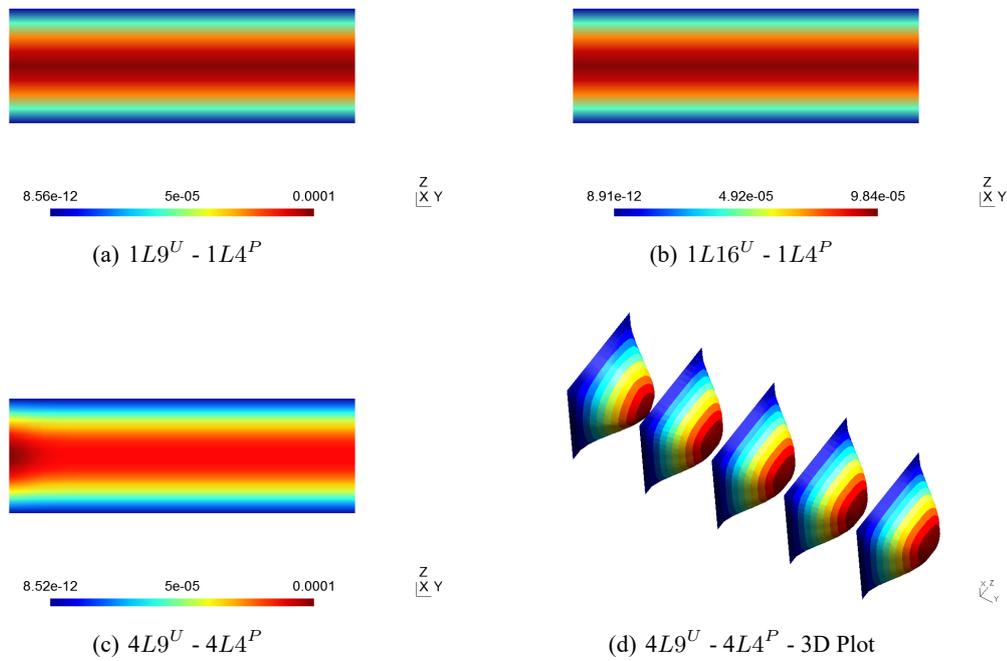(d) $4L9^U$ - $4L4^P$ - 3D Plot

Fig. 13 Axial velocity u_y in square-section pipe. Comparison of three different models (a),(b),(c), values are in [m/s]; 3D plot of u_y of $4L9^U 4L4^P$ model (d)

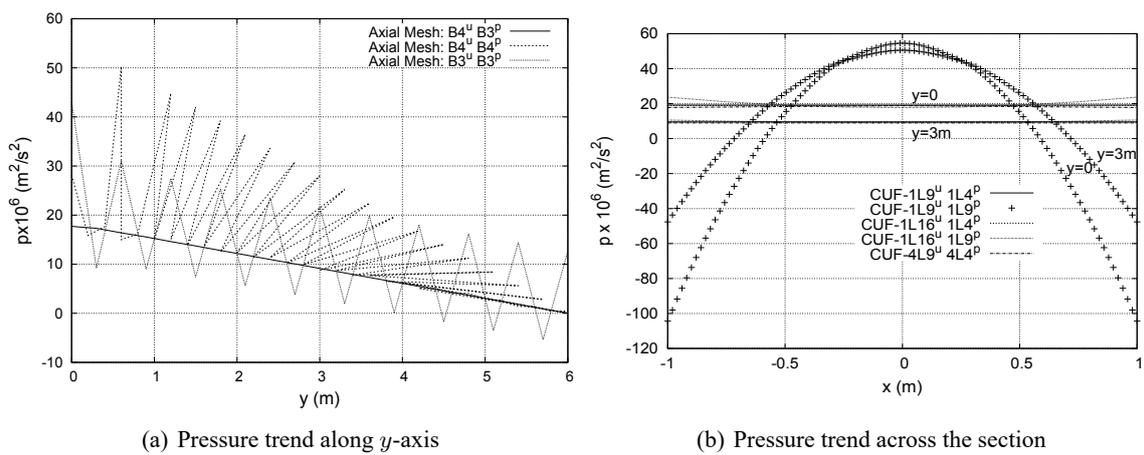(a) Pressure trend along y-axis

(b) Pressure trend across the section

Fig. 14 Pressure trend comparison: (a) models with different FE order of the y-axis (b) models with different order of expansion across the section

employed for the description of the flow in both circular and square section conduct. The results obtained from these 1D models have been compared with the analytical solution and with 3D numerical approximations obtained via finite volume software OpenFoam. The analysis here performed clearly underlines:

- LE and TE models based on CUF provide accurate results of velocity and pressure with respect to analytical solution.

- 1D models allow to obtain efficient results with lower computational costs compared with those obtained via 3D finite volume software.

- CUF represents an alternative tool to investigate the Stokes flow also in non-circular section cylinders.

These promising preliminary results can be considered as a first step toward more advanced applications, like complex fluids and fluid-structure interaction.

References

Brezzi, F. (1974), "On the existence, uniqueness and approximation of saddle-point problems arising from Lagrange multipliers", *Revue Francaise de Automatique, Informatique, Recherche Operationnelle. Analyse Numerique*, **8**,129-151.

Carrera, E., Petrolo, M. and Varello, A. (2012), "Advanced beam formulations for free-vibration analysis of conventional and joined wings", *J. Aerosp. Eng.*, **25**(2), 282-293.

Carrera, E. and Pagani,A. (2014), "Free vibration analysis of civil engineering structures by component-wise models", *J. Sound Vibr.*, **333**(19), 4597-4620.

Carrera, E. and Giunta, G. (2010), "Refined beam theories based on a unified formulation", *Int. J. Appl. Mech.*, **2**(1), 117-143.

Carrera, E. and Petrolo, M. (2012), "Refined beam elements with only displacement variables and plate/shell capabilities", *Meccan.*, **47**(3), 537-556.

Carrera, E., and Cinefra, M., Petrolo, M. and Zappino, E. (2014), *Finite Element Analysis of Structures Through Unified Formulation*, John Wiley & Sons Ltd.

Carrera, E. and Zappino, E. (2017), "One-dimensional finite element formulation with node-dependent kinematics", *Comput. Struct.*, **192**(1), 114-125.

Carrera, E., Cinefra, M., Petrolo, M. and Zappino, E. (2014), *Finite Element Analysis of Structures through Unified Formulation*, John Wiley & Sons Ltd.

Euler, L. (1775) *Principia Pro Motu Sanguinis Per Arterias Determinando*.

Fung, Y.C. (1997), *Biomechanics: Circulation*, Springer.

Filippi, M. and Carrera, E. (2016), "Capabilities of 1d cuf-based models to analyse metallic/composite rotors" *Adv. Aircraft Spacecraft Sci.*, **3**(1), 1-14.

Formaggia, L., Gerbeau, J.F., Nobile, F. and Quarteroni, A. (2001), "On the coupling of 3d and 1d Navier-Stokes equations for flow problems in compliant vessels", *Comput. Meth. Appl. Mech. Eng.*, 561-582.

Formaggia, L., Lamponi, D. and Quarteroni, A. (2003), "One-dimensional models for blood flow in arteries", *J. Eng. Math.*, 251-279.

Giunta, G., Biscani, F., Belouettar, S., Ferreira, A.J.M. and Carrera, E. (2013), "Free vibration analysis of composite beams via refined theories", *Compos. Part B: Eng.*, **44**(1), 540-552.

Miglioretti, F. and Carrera, E. (2015), "Application of a refined multi-field beam model for the analysis of complex configurations", *Mech. Adv. Mater. Struct.*, **22**(1-2), 52-66.

OpenFOAM Fundation (2011), *OpenFOAM*, <www.openfoam.com>.

Pagani, A. (2015) "Component-wise models for static,dynamic and aeroelastic analyses of metallic and composite aerospace structures", Ph.D. Dissertation, Politecnico di Torino, Italy.

Pagani, A., De Miguel, A., Petrolo, M. and Carrera, E. (2016), "Analysis of laminated beams via unified formulation and legendre polynomial expansions", *Compos. Struct.*, **156**, 78-92 .

Perotto, S., Ern, A. and Veneziani, A. (2009), "Hierarchical local model reduction for elliptic problems i: A domain decomposition approach", *A SIAM Interdiscipl. J.*, **8**, 1102-1127.

Perotto, S., Reali, A., Rusconi, P. and Veneziani, A. (2017), " Higamod: A hierarchical isogeometric approach for {MODel} reduction in curved pipes", *Comput. Flu.*, **142**, 21-29.

Quarteroni, A., Formaggia, L. and Veneziani, A. (2009), *Cardiovascular Mathematics*, **1**.

Quarteroni, A. and Rozza, G. (2006), "Numerical solution of parametrized navier-stokes equations by reduced basis methods", *Numer. Meth. Part. Differ. Eq.*, 923 -948.

Quarteroni, A. (2009), *Numerical Models for Differential Problems*, Springer.

Ravindran, S.S. (2000), "Reduced-order approach for optimal control of fluids using proper orthogonal decomposition", *Int. J. Numer. Meth. Flu.*

Stera, S. and Skalak, R. (1993), *The History of Poiseuille's Law*.

Salmoiraghi, F., Ballarin, F., Heltai, L. and Rozza, G. (2016), "Isogeometric analysis-based reduced order modelling for incompressible linear viscous flows in parametrized shapes", *Adv. Model. Simul. Eng. Sci.*, 3-21 .

Smith, N.P., Pullan, A.J. and Hunter, P.J. (2002), "An anatomically based model of transient coronary blood flow in the heart", *SIAM J. Appl. Math.*, 990-1018.

Sherewin, S.J., Franke, V. and Peiro, J. (2003), "One-dimensional modelling of a vascular network in space-time variables", *J. Eng. Math.*, 217-250 .

Vreugdenhil, C.B. (1998), *Numerical Methods for Shallow/Water Flows*.

Varello, A. (2013), "Advanced higher-order one-dimensional models for fluid-structure interaction analysis", Ph.D. Dissertation, Politecnico di Torino, Italy.

Zienkiewicz, O.C. and Taylor, R.L. (1977), *The Finite Element Method*, McGraw-Hill, London, U.K.

EC